Detection & location of earthquakes in Canadian Rocky Mountain Trench by kurtosis & Bayesian sampling in the presence of strong cultural noise

Poster
S31C-0512

joshua.purba@ucalgary.ca

Joshua Purba, Hersh Gilbert, and Jan Dettmer

Department of Geoscience, University of Calgary

UNIVERSITY OF CALGARY

Introduction

To improve our understanding of the Canoe Reach Geothermal Field in the Rocky Mountain Trench of western Canada, we study local earthquakes in the area. By investigating its seismicity, we seek to constrain the structure and movement of the Rocky Mountain Trench. This area exhibits mountainous terrain and strong cultural noise from communities, roads and trains that makes detecting earthquakes challenging. To compile an earthquake catalog from a 4-month recording on 10 broadband stations, we employ two independent detection methods, STA/LTA and kurtosis. The approach detects 19 local events as well as many regional and teleseismic events. We focus on 9 local events with high SNR and carry out Bayesian uncertainty quantification of their locations. The inversion considers both location of individual events and joint inversion for multiple earthquakes and includes rigorous hierarchical treatment of picking errors. Jointly locating substantially reduces location uncertainty. The locations reveal two doublets from two different locations.

Dataset

Data are from 10 broadband 3-component seismometers deployed in 2017 near the Canoe Reach Geothermal Field in Valemount, British Columbia. The sampling rate is 50 Hz and we consider data from September to December 2017. The area hosts the Rocky Mountain Trench which is a major structure that spans much the eastern Canadian Cordillera, yet remains poorly understood.

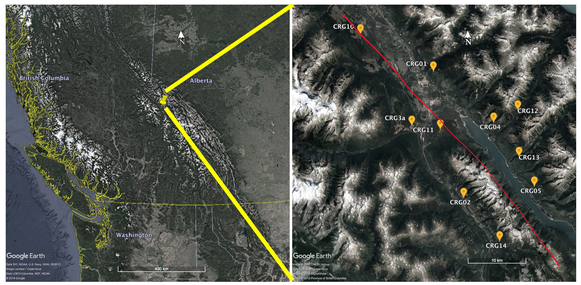

(a) (b)

Figure 1: (a) Regional map of western Canada. (b) Local map of the 10-seismometer array near Valemount, B.C. We approximate the location of the trench by the red line in (b).

Detection Method

STA/LTA detection is widely applied to seismic data and utilizes the ratio of long-time-average (LTA) to short-time average (STA) of the signal. It applies a threshold to trigger the detection.

Kurtosis is a statistical moment representing the distribution tail and is insensitive to emerging signals but more sensitive to impulsive earthquake onsets. Here, a dynamic threshold is applied for kurtosis: $\mu + \theta * \sigma$, where μ is signal mean, θ is a subjective parameter, and σ is the signal standard deviation *(Paes & Eaton, 2018)*. Both methods use the same number of channel declarations and normal moveout correction values.

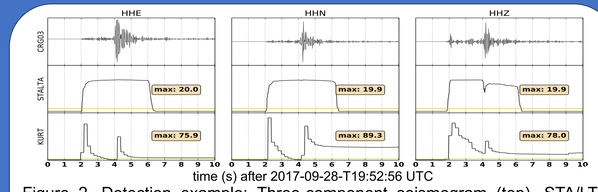

Figure 2. Detection example: Three-component seismogram (top), STA/LTA characteristic function (middle), and Kurtosis exceedance (bottom). A bandpass filter of 10-20 Hz is applied. Both methods detect the earthquake clearly.

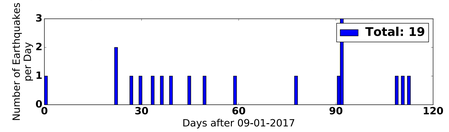

Figure 3. The 19 local events detected during September to December 2017. Two doublets were detected during this period.

Location Method: 2 Doublets Detected

Bayesian inference is applied via MCMC sampling to manual P- and S- arrival picks. The inversion treats origin times, locations, half-space velocities, and picking errors for P- and S- arrivals as unknown parameters. MCMC sampling is applied efficiently with a proposal distribution in principal component space (*Dettmer et al., 2007*). Results are considered in terms of 1D and 2D marginal distributions. Here we compare single-event locations with locating multiple events jointly.

Doublet 1

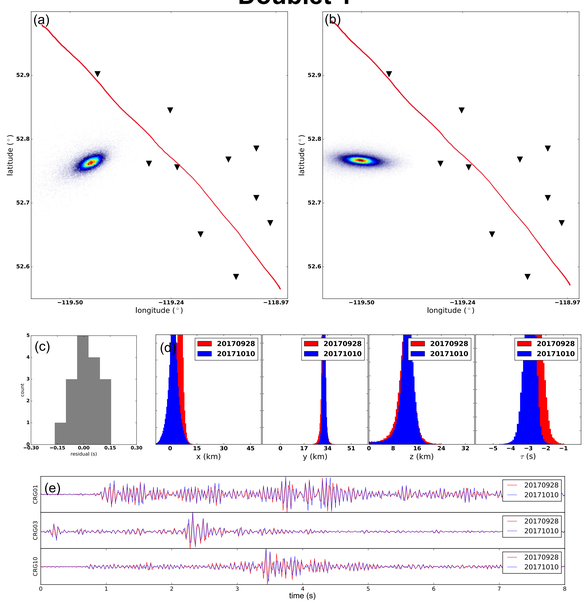

Figure 4. (a-b) Location maps for doublet 1 (events 2017-09-28 and 2017-10-10). (c) P- and S-pick residuals for 2017-09-28 appear reasonable. (d) Location uncertainties for both earthquakes identify these events as a doublet. (e) Vertical-component waveforms for doublet 1 at three stations; event 2017-09-28 (red) match closely those of event 2017-10-10 (blue).

Doublet 2

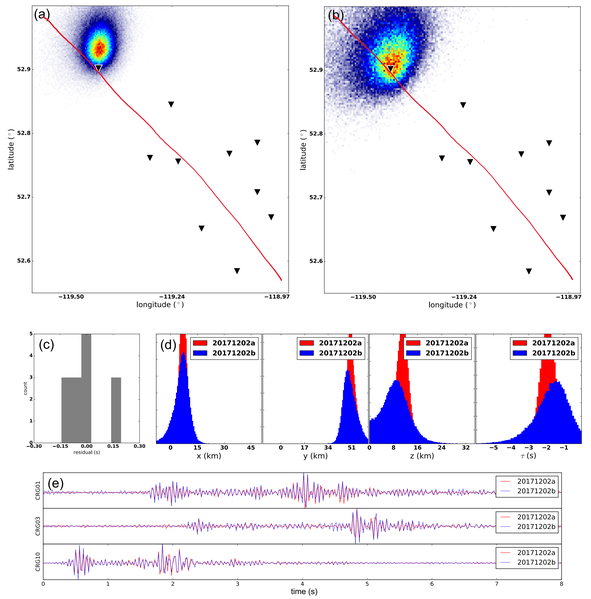

Figure 5. (a-b) Location maps for doublet 2 (events 2017-12-02a and 2017-12-02b). (c) P- and S-pick residuals for 2017-09-28 appear reasonable but these events exhibit lower SNR compared to doublet 1. (d) Location uncertainties for both earthquakes show that these events originate in close proximity. Note that origin times are separated by only 15 hours. (e) Vertical-component waveforms for doublet 1 at three stations; event 2017-12-2a (red) match closely those of event 2017-12-2b (blue).

Joint Inversion Results

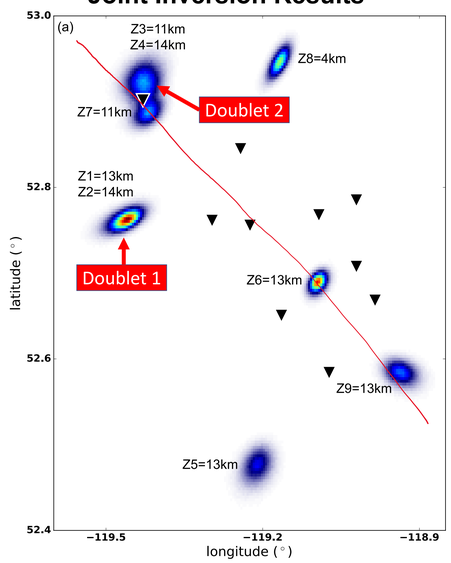

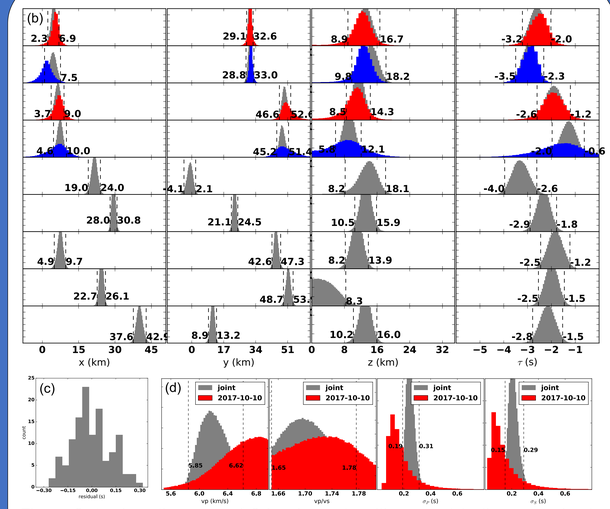

Figure 6. (a) Location map of 9 local events with respect to the approximate surface trace of the trench. Depth for each event is plotted. (b) Residuals from the joint-inversion appear reasonable and suggest no inconsistent information between events. (c) 1D marginal distributions for joint inversion of 9 events compared to individual inversions of 4 events. Dash lines are the 95% Credibility Intervals. Joint inversion substantially reduces location uncertainty. (d) Comparison of hierarchical parameters (Vp, Vp/Vs ratio, and two noise parameters) for single-event and joint inversions. The joint inversion substantially improves average crustal velocity estimates

Discussion

Our study identifies **two sets of event doublets**. Examples of their waveforms are shown in Figures 4e & 5e. The time separation between the events in each of these doublets is 12 days and 15 hours, respectively. For both doublets, location results show origin estimates that nearly perfectly align in terms of 95% Confidence Interval (CI) (Fig. 6). Similar doublets have been documented along the San Andreas Fault system and attributed to the migration of fluids through the fault zone. The presence of doublets in this area of the Rocky Mountain Trench may indicate that fluids also play a role in generating this seismicity. Further investigation into this seismicity will explore links between seismicity and the Canoe Reach Geothermal Field.

The **Bayesian method** provides rigorous location uncertainties for 9 events. Compared to single-event inversion, the joint inversion substantially reduces uncertainty. In addition to location parameters, the method treats average crustal P-wave velocity and Vp/Vs ratio as unknown. The prior bounds for these parameters are based on literature estimates (*Clowes et al., 2005*). The 95% CI for Vp is 5.85-6.62 km/s, the 95% CI Vp/Vs estimate is 1.65-1.78, and the 95% CI for the depths of the events range between 8.2 to 18.2 km. Future work will extend this study by jointly inverting a larger number of events and carrying out our analysis on the full year of recorded data.

Acknowledgments:

We acknowledge support from NSERC Discovery Grants to H. Gilbert and J. Dettmer. Support from Nanometrics and Borealis Geopower facilitated the data acquisition. We thank our colleagues in the seismology group at the University of Calgary for providing helpful feedback and guidance for this study.

References:

A. Paes and D. Eaton (2018), Proceedings of Microseismic Industry Consortium Conference.

J. Dettmer et al (2007), Journal of the Acoustical Society of America.

R.M. Clowes et al (2005), Canadian Journal of Earth Sciences.